**Supplementary Information**

# Chemoreceptor TRPγ coordinates locomotor activity via regulating intracellular $Ca^{2+}$ homeostasis in *Drosophila*

Peiyuan Pang[1,#], Bomin Gao[1,#], Xiaoyi Mo[1,#], Xuteng Lu[1,#], Xiang Li[2], Peiyu Wang[1], Qiong Shi[1], Keyu Xia[1], Panhao Xiao[1], Hongcun Gai[1], Chang Xie[1], Dongdong Li[3,4], Demeng Sun[2,*], Changlin Tian[2,*], Jing Yao[1,*]

[1] State Key Laboratory of Virology and Biosafety, Hubei Provincial Research Center for Basic Biological Sciences, College of Life Sciences, TaiKang Center for Life and Medical Sciences, Hubei Key Laboratory of Cell Homeostasis, Frontier Science Center for Immunology and Metabolism, Wuhan University, Wuhan, Hubei 430072, China

[2] Hefei National Laboratory for Physical Sciences at the Microscale, Division of Life Sciences and Medicine, University of Science and Technology of China, Hefei 230026, P. R. China

[3] Sorbonne Université, CNRS, Inserm, Neuro-SU, F-75005 Paris, France France

[4] Sorbonne Université, CNRS, Inserm, Institut de Biologie Paris-Seine, IBPS, F-75005 Paris, France

# These authors contributed equally to this work.

* Corresponding authors. Email: jyao@whu.edu.cn; cltian@ustc.edu.cn and dmsun@ustc.edu.cn

**This file includes:**

Extended Data Fig. 1 to 8

Extended Data Tables 1 to 2

# Extended Data

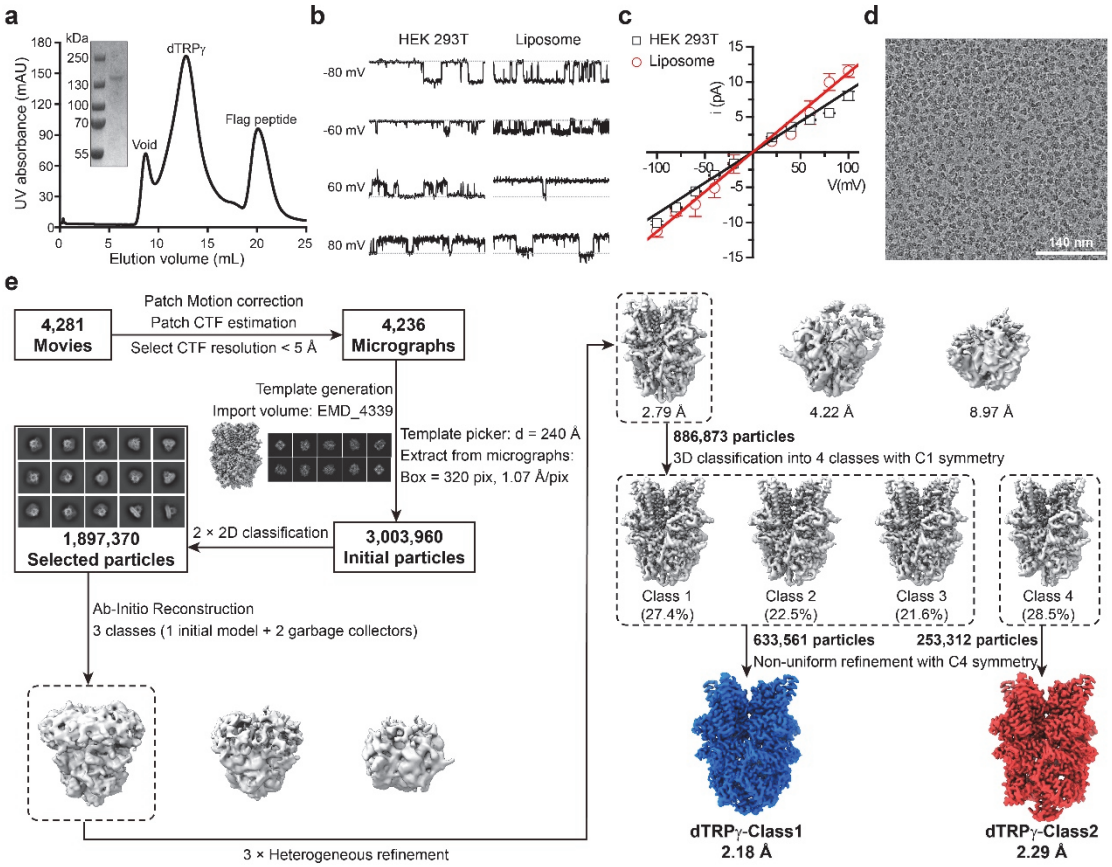


**Extended Data Fig. 1 | Protein purification and Cryo-EM data processing of dTRPγ.**

**a**, Purification of the *drosophila* TRPγ protein, representative size-exclusion chromatography and SDS-PAGE analysis. Peaks corresponding to void, dTRPγ tetramer, and Flag peptide are indicated. **b**, Representative single-channel currents of dTRPγ recorded from outside-out membrane patches of HEK 293T cells (left) or proteoliposome (right) evoked by 3 mM camphor at the indicated holding potentials after sensitization. Dotted lines indicate the closed channel state. **c**, Plot of unitary current amplitudes versus voltages. Note that the unitary currents were determined by fitting all-point histograms with Gaussians. **d**, Representative cryo-EM micrograph from 4,281 movies (scale bar, 140 nm). **e**, Cryo-EM data processing workflows of

dTRPγ. Dashed boxes indicate selected classes. Representative 2D class averages and 3D reconstruction refinements are displayed along with global Gold-standard Fourier Shell Correlation (GSFSC) resolutions.

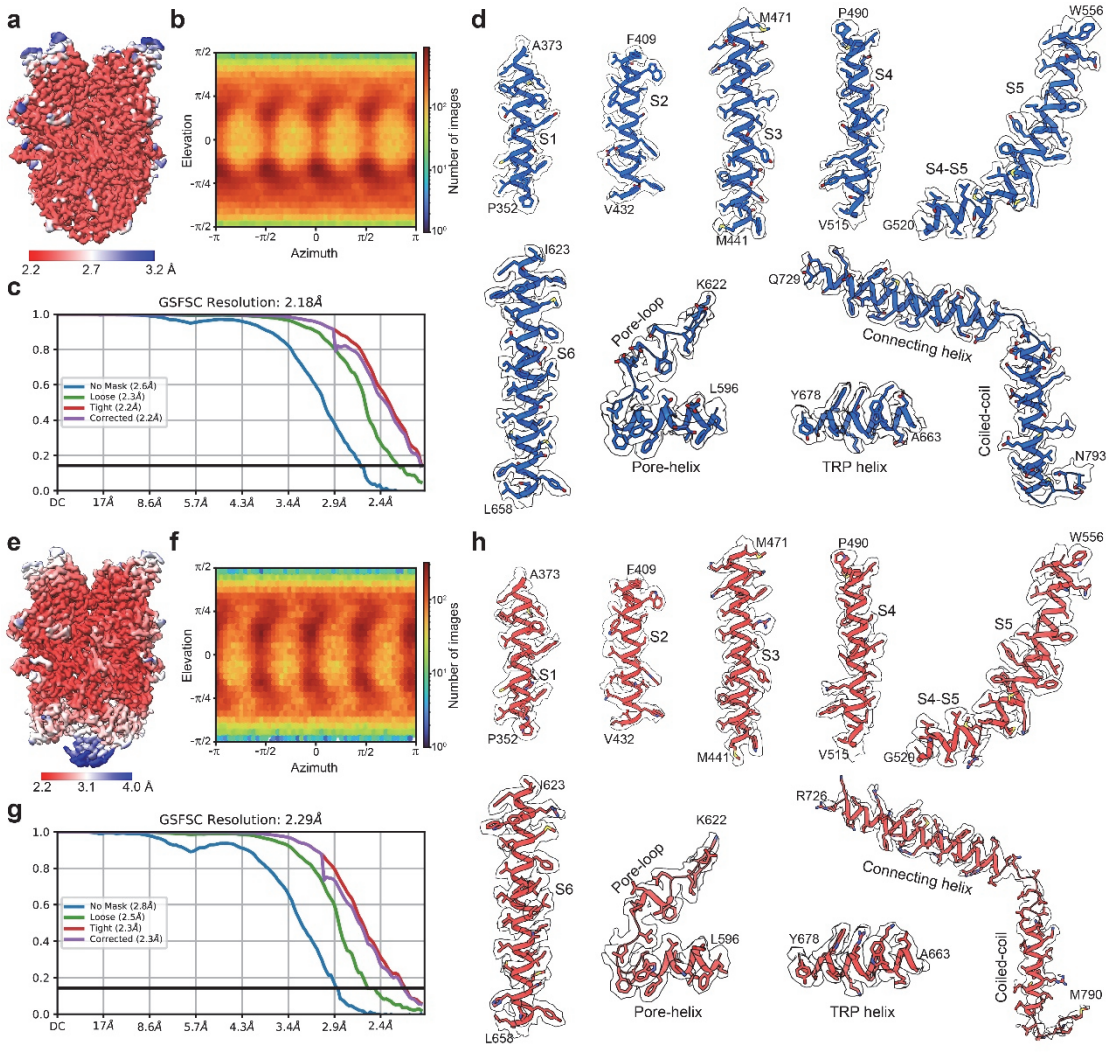


**Extended Data Fig. 2 | Local resolution and characteristics of dTRPγ cryo-EM reconstructions.**

**a**, Local resolution estimation of the dTRPγ-Class1 reconstruction, color-coded from 2.2 Å (red) to 3.2 Å (blue). **b**, Angular distribution of particle orientations for dTRPγ-Class1. This is a standard output from cryoSPARC. **c**, Fourier Shell Correlation (FSC) curves of final refinement for dTRPγ-Class1 calculated between half maps, with the overall resolution of 2.18 Å estimated using the FSC = 0.143 criterion. **d**, Representative cryo-EM densities of transmembrane helices (S1-S6), pore domain, TRP helix and coiled-coil domain in dTRPγ-Class1 reconstruction. **e**, Local resolution

estimation of the dTRPγ-Class2 reconstruction, color-coded from 2.2 Å (red) to 4.0 Å (blue). **f**, Angular distribution of particle orientations for dTRPγ-Class2. This is a standard output from cryoSPARC. **g**, Fourier Shell Correlation (FSC) curves of final refinement for dTRPγ-Class2 calculated between half maps, with the overall resolution of 2.29 Å estimated using the FSC = 0.143 criterion. **h**, Representative cryo-EM densities of transmembrane helices (S1-S6), pore domain, TRP helix and coiled-coil domain in dTRPγ-Class2 reconstruction.

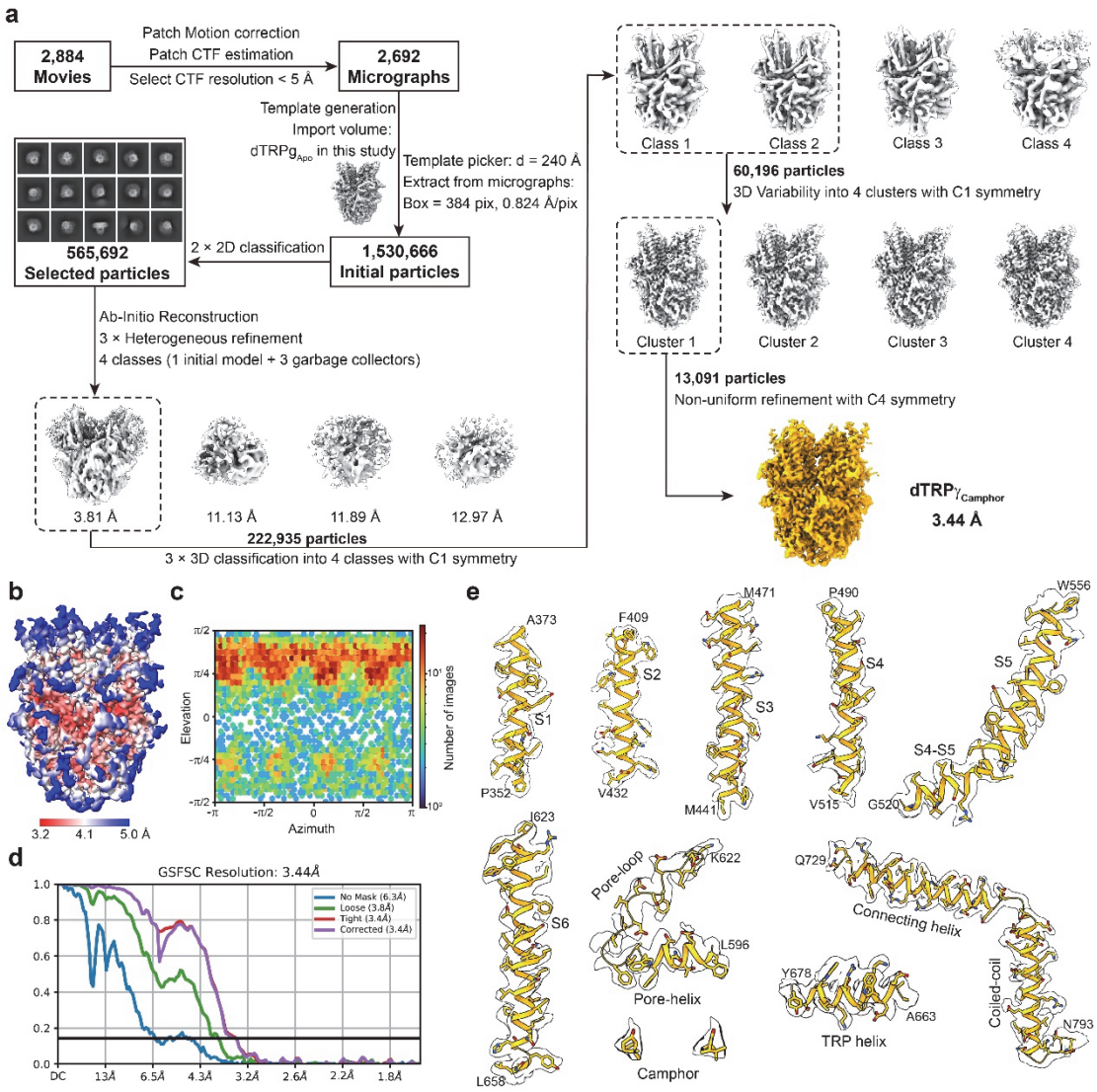


**Extended Data Fig. 3 | Cryo-EM data processing, local resolution and characteristics of dTRPγ$_{Camphor}$ reconstruction.**

**a**, Cryo-EM data processing workflow of dTRPγ$_{Camphor}$. Dashed boxes indicate selected classes. Representative 2D class averages and 3D reconstruction refinements are displayed along with global Gold-standard Fourier Shell Correlation (GSFSC) resolutions. **b**, Local resolution estimation of the dTRPγ$_{Camphor}$ reconstruction, color-coded from 3.2 Å (red) to 5.0 Å (blue). **c**, Angular distribution of particle orientations for dTRPγ$_{Camphor}$. This is a standard output from cryoSPARC. **d**, Fourier Shell Correlation (FSC) curves of final refinement for dTRPγ$_{Camphor}$ calculated between half

maps, with the overall resolution of 3.44 Å estimated using the FSC = 0.143 criterion. **e**, Representative cryo-EM densities of transmembrane helices (S1-S6), pore domain, camphor, TRP helix and coiled-coil domain in dTRP$\gamma_{Camphor}$ reconstruction.

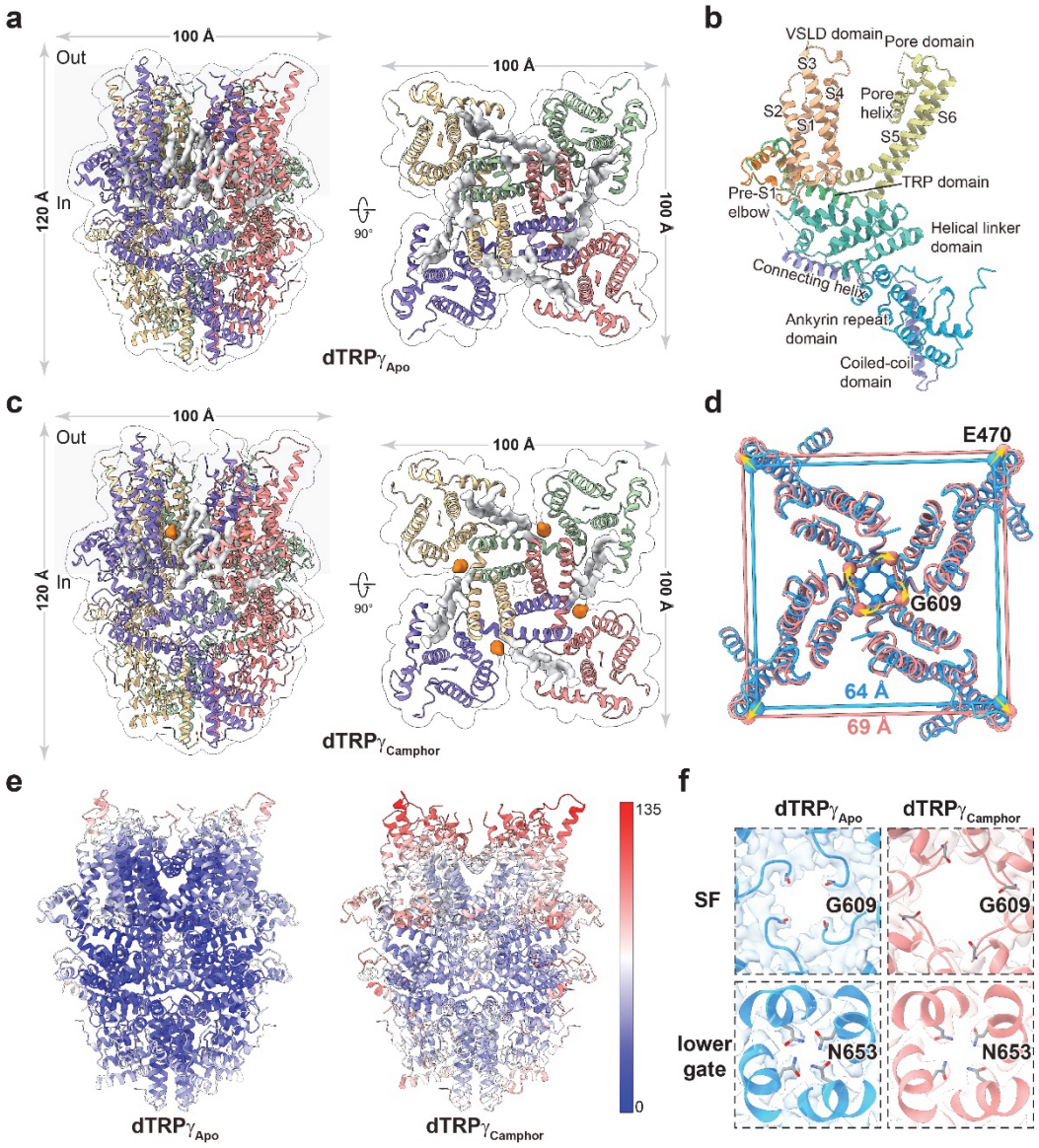


**Extended Data Fig. 4 | Structural comparisons of dTRPγ$_{Apo}$ and dTRPγ$_{Camphor}$.**

**a**, Ribbon diagrams of dTRPγ$_{Apo}$ atomic model with channel dimensions indicated. Each of the four identical subunits is color-coded, showing views from side (left) and top (right). The lipids are rendered as gray surfaces. **b**, Ribbon diagrams depicting structural details of a single subunit, color-mapped to distinct structural regions as indicated. **c**, Ribbon diagrams of dTRPγ$_{Camphor}$ atomic model. Subunit coloring and lipids rendering match panel (a). **d**, Structural superposition of the transmembrane domains from apo (blue) and camphor-bound (red) states. Carbon backbones of G609

and E470 are represented as spheres, with yellow arrows indicating displacement vectors. Adjacent subunit distance changes (Å) between E470 residues (connected by solid lines) are annotated. **e**, Ribbon representation of dTRP$\gamma_{Apo}$ (left) and dTRP$\gamma_{Camphor}$ (right) structure colored by B-factor (scale: 0–135 Å$^2$), with lower values (blue) indicating rigid regions and higher values (red) corresponding to flexible regions. **f**, Top views of the selectivity filter (SF) and the lower gate in dTRP$\gamma_{Apo}$ (blue) and dTRP$\gamma_{Camphor}$ (red), corresponding amino acid residues (G609 for SF and N653 for lower gate) are shown as sticks.

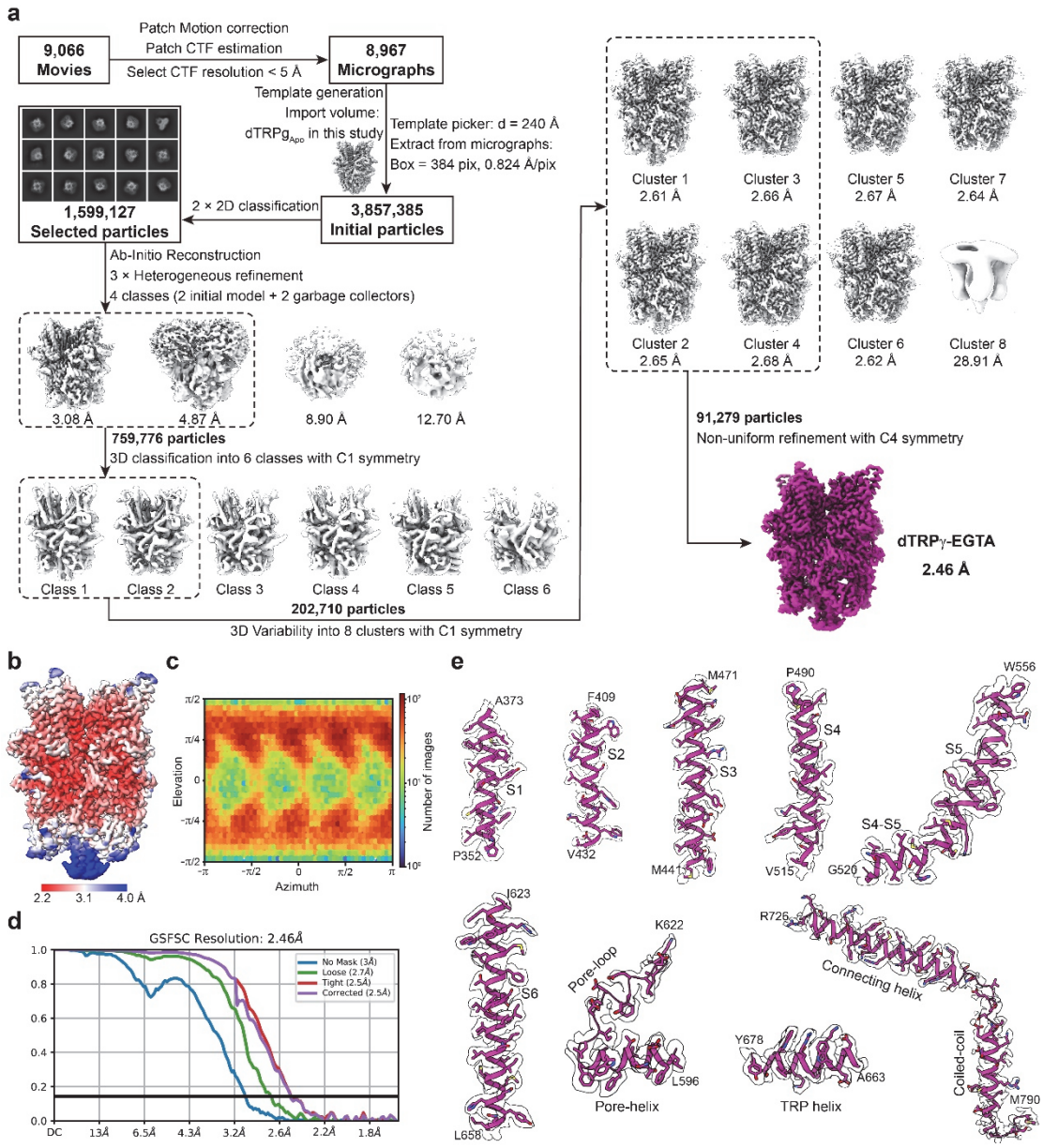


**Extended Data Fig. 5 | Cryo-EM data processing, local resolution and characteristics of dTRPγ-EGTA reconstruction.**

**a**, Cryo-EM data processing workflow of dTRPγ-EGTA. Dashed boxes indicate selected classes. Representative 2D class averages and 3D reconstruction refinements are displayed along with global Gold-standard Fourier Shell Correlation (GSFSC) resolutions. **b**, Local resolution estimation of the dTRPγ-EGTA reconstruction, color-coded from 2.2 Å (red) to 4.0 Å (blue). **c**, Angular distribution of particle orientations

for dTRPγ-EGTA. This is a standard output from cryoSPARC. **d**, Fourier Shell Correlation (FSC) curves of final refinement for dTRPγ-EGTA calculated between half maps, with the overall resolution of 2.46 Å estimated using the FSC = 0.143 criterion. **e**, Representative cryo-EM densities of transmembrane helices (S1-S6), pore domain, TRP helix and coiled-coil domain in dTRPγ-EGTA reconstruction.

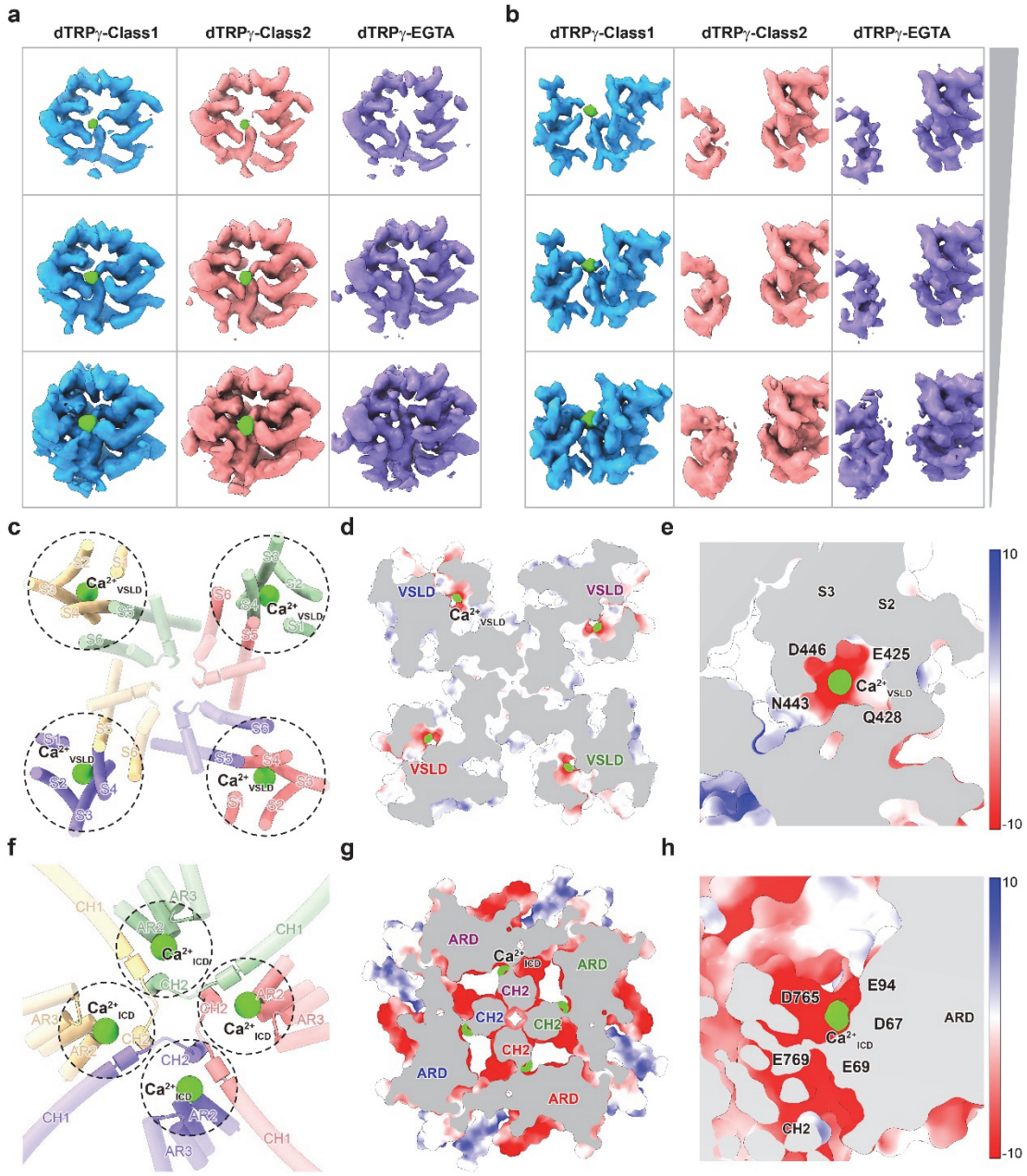


**Extended Data Fig. 6 | Structural characterization of $Ca^{2+}$-binding sites in dTRPγ.** **a-b,** Cryo-EM densities of the $Ca^{2+}_{VSLD}$ **(a)** and $Ca^{2+}_{ICD}$ **(b)**-binding sites in dTRPγ-Class1 (blue), dTRPγ-Class2 (red) and dTRPγ-EGTA (purple) contoured at decreasing levels from top to bottom panels. The densities of $Ca^{2+}$ are presented as green surfaces. Density visualization performed in UCSF ChimeraX. **c**, Top-view architecture of the tetrameric transmembrane domain (TMD) with dashed circles highlighting $Ca^{2+}_{VSLD}$ (green spheres)-binding sites. **d-e**, Electrostatic potential surfaces (scale in kcal

$mol^{-1}e^{-1}$) of the $Ca^{2+}_{VSLD}$-binding sites viewed from the top **(d)** and the zoomed-in view **(e)**. **f**, Top-view architecture of the tetrameric intracellular domain (ICD) with dashed circles highlighting $Ca^{2+}_{ICD}$ (green spheres)-binding sites. **g-h**, Electrostatic potential surfaces (scale in kcal $mol^{-1}e^{-1}$) of the $Ca^{2+}_{ICD}$-binding sites viewed from the top **(g)** and the zoomed-in view **(h)**.

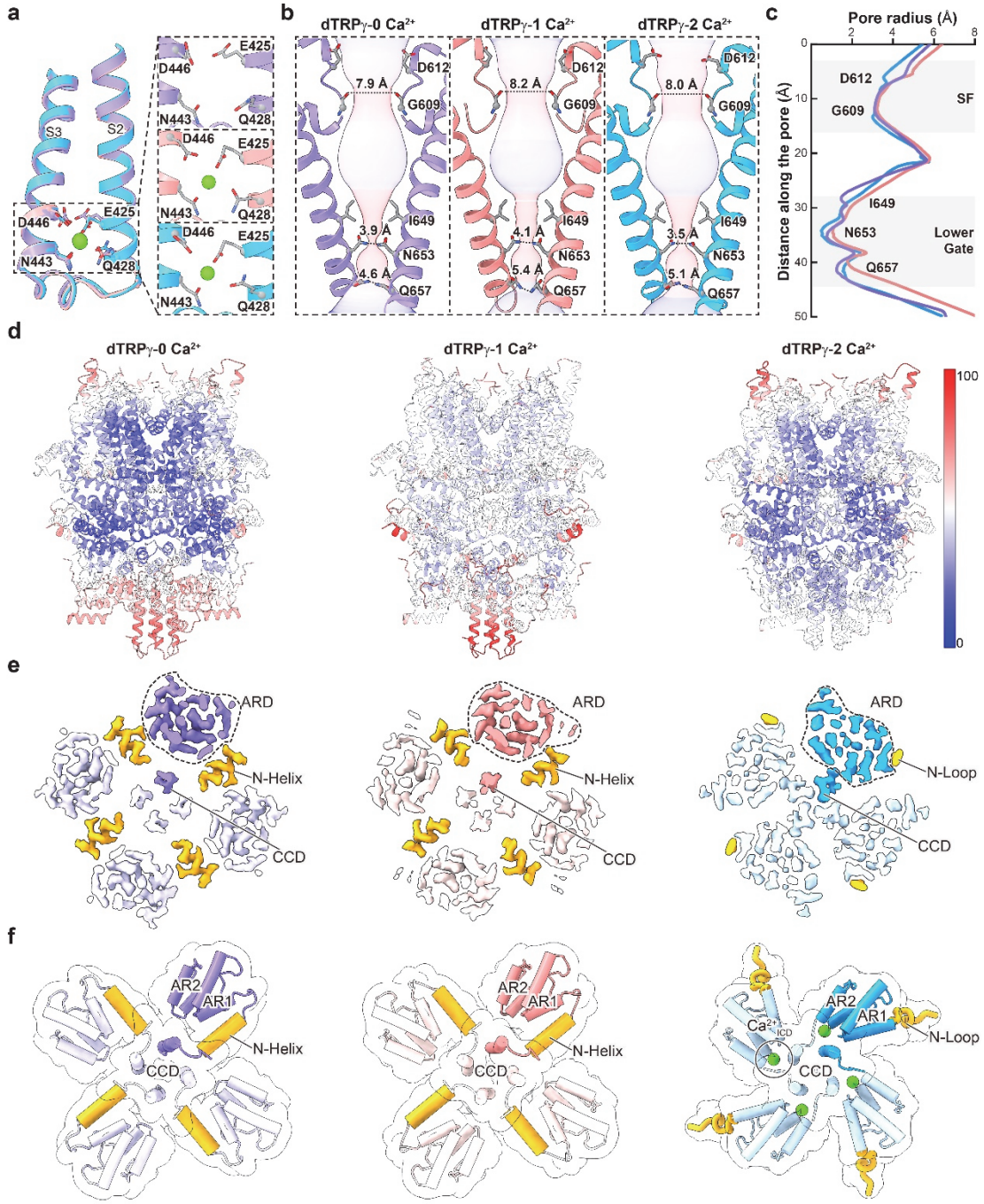


**Extended Data Fig. 7 | $Ca^{2+}$-binding induced conformational changes of dTRPγ.**

**a,** Structural comparison of the VSLD in dTRPγ-0 $Ca^{2+}$ (purple), dTRPγ-1 $Ca^{2+}$ (red) and dTRPγ-2 $Ca^{2+}$ (blue), with close-up views (dashed box) showing conformational changes upon $Ca^{2+}$ binging. **b**, Profiles of ion-conduction pores (shown as a surface representation) in dTRPγ-0 $Ca^{2+}$ (purple), dTRPγ-1 $Ca^{2+}$ (red) and dTRPγ-2 $Ca^{2+}$ (blue), calculated with MOLE. The pore region (shown as cartoon) and residues (shown as

sticks) forming the gate and the selectivity filter in two opposing subunits are depicted. Diagonal distances between gating residues are annotated. **c**, Quantitative pore radius along the central axis corresponding to **(b)**. **d**, Ribbon representation of dTRPγ-0 $Ca^{2+}$ (left), dTRPγ-1 $Ca^{2+}$ (middle) and dTRPγ-2 $Ca^{2+}$ (right) structure colored by B-factor (scale: 0–100 $Å^2$), with lower values (blue) indicating rigid regions and higher values (red) corresponding to flexible regions. **e**, Cross-sectional cryo-EM maps of ICD in dTRPγ-0 $Ca^{2+}$ (purple), dTRPγ-1 $Ca^{2+}$ (red) and dTRPγ-2 $Ca^{2+}$ (blue), viewed from bottom. The ARD of one subunit is circled by a dashed line with N-Helix and N-Loop highlighted in yellow. **f**, Cartoon models of ICD corresponding to **(e)**.

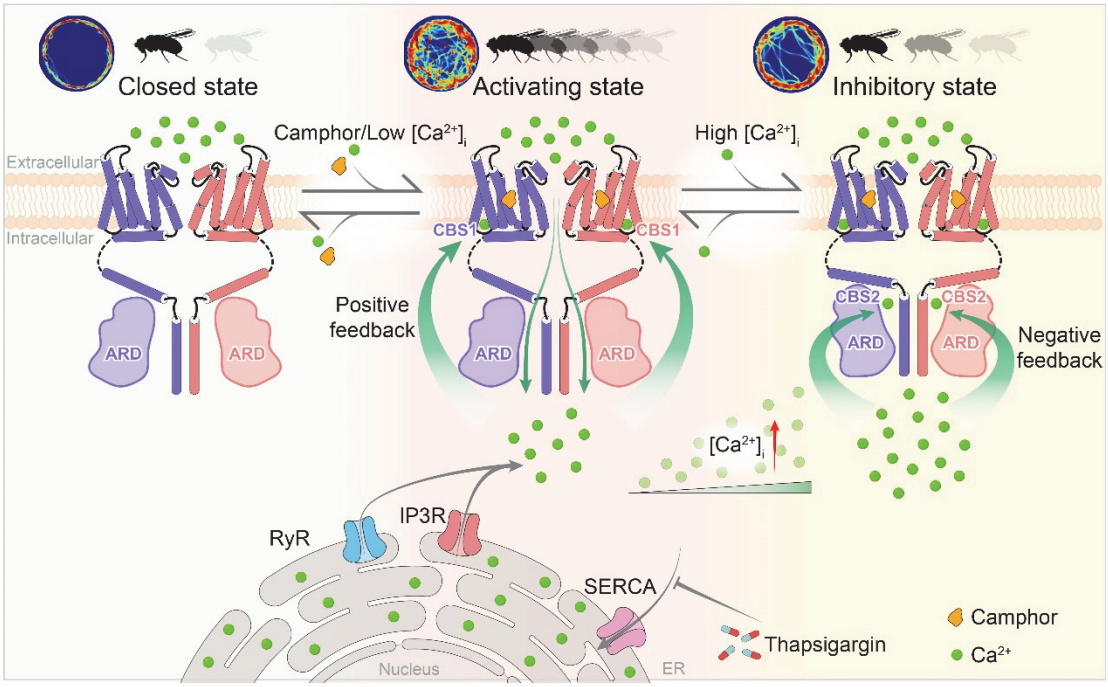


**Extended Data Fig. 8 | Schematic of the molecular mechanisms underlying bidirectional regulation of dTRPγ.**

Camphor binds to an orthosteric pocket formed by adjacent subunits within TMD, triggers pore rearrangement, thereby activating dTRPγ and mediating the influx of $Ca^{2+}$. At low $[Ca^{2+}]_i$, $Ca^{2+}$ binding to CBS1 activates the channel and promotes $Ca^{2+}$ influx (Positive feedback). At elevated $[Ca^{2+}]_i$, $Ca^{2+}$ binding to CBS2 sterically blocks ion permeation via enclosing the tunnel of cation pathway towards the cytosol (Negative feedback). This bidirectional autoregulatory circuit dynamically maintains intracellular calcium homeostasis. In addition, $Ca^{2+}$ release via RyR and IP3R on the endoplasmic reticulum and the $[Ca^{2+}]_i$ elevation triggered by thapsigargin-mediated SERCA inhibition directly regulate dTRPγ channel function. *In vivo*, dTRPγ acts as a chemo-electrical transducer integrating environmental cues with ionic dynamics, contributing to the locomotor activity of *Drosophila*. CBS: Calcium Binding Site; ARD: Ankyrin Repeat Domain.

**Extended Data Table 1. Primers for construction of dTRPγ mutants**

| ID | Primer Name | Primer Sequence (from 5′ to 3′) |
|---|---|---|
| 1 | dTRPg_F504A_F | GTGCAGCGAACATTGCCAGTAGCCTCAAGC |
| 2 | dTRPg_F504A_R | GCTTGAGGCTACTGGCAATGTTCGCTGCAC |
| 3 | dTRPg_L507S_F | GCAGCGAACATTTTCAGTAGCAGCAAGCTGGTTTATATATTCTC |
| 4 | dTRPg_L507S_R | GAGAATATATAAACCAGCTTGCTGCTACTGAAAATGTTCGCTGC |
| 5 | dTRPg_V543T_F | CTTCTTTTTATATGTCCTAACCCTGTTCGCTTTTGGCAG |
| 6 | dTRPγ_V543T_R | CTGCCAAAAGCGAACAGGGTTAGGACATATAAAAAGAAG |
| 7 | dTRPγ_F547A_F | CTAGTCCTGTTCGCTGCAGGCAGTGGTCTCAATC |
| 8 | dTRPγ_F547A_R | GATTGAGACCACTGCCTGCAGCGAACAGGACTAG |
| 9 | dTRPγ_T635A_F | GGGCATGCTAATGTTTGGAGCCTACTCGGTCATAAATATTG |
| 10 | dTRPγ_T635A_R | CAATATTTATGACCGAGTAGGCTCCAAACATTAGCATGCCC |
| 11 | dTRPγ_I639F_F | GTTTGGAACTTACTCGGTCTTCAATATTGTGGTGCTGCTC |
| 12 | dTRPγ_I639F_R | GAGCAGCACCACAATATTGAAGACCGAGTAAGTTCCAAAC |
| 13 | dTRPγ_E425Q_F | GTCTCATCTGGAGCCAGGTGAAGCAACTG |
| 14 | dTRPγ_E425Q_R | CAGTTGCTTCACCTGGCTCCAGATGAGAC |
| 15 | dTRPγ_D446N_F | CATGTGGAATGTGATCAACTTTGTCACGAACTC |
| 16 | dTRPγ_D446N_R | GAGTTCGTGACAAAGTTGATCACATTCCACATG |
| 17 | dTRPγ_D765N_F | GGGAGTCACCGAGAACGATGTGAATGAG |
| 18 | dTRPγ_D765N_R | CTCATTCACATCGTTCTCGGTGACTCCC |
| 19 | dTRPγ_D612N_F | GTCTTCGGCCTAATCAACTTGGACAGCTTTGAGTTGG |
| 20 | dTRPγ_D612N_R | CCAACTCAAAGCTGTCCAAGTTGATTAGGCCGAAGAC |

**Extended Data Table 2. Cryo-EM data collection, refinement and validation statistics**

| | dTRPγ- Class1 (EMD-65273) (PDB 9VQQ) | dTRPγ- Class2 (EMD-65279) (PDB 9VQW) | dTRPγ-EGTA (EMD-65280) (PDB 9VQX) | $dTRP\gamma_{Camphor}$ (EMD-65281) (PDB 9VQY) |
|---|---|---|---|---|
| **Data collection and processing** | | | | |
| Magnification | 81,000 | 81,000 | 105,000 | 105,000 |
| Voltage (kV) | 300 | 300 | 300 | 300 |
| Electron exposure (e–/Å$^2$) | 50 | 50 | 50 | 50 |
| Defocus range (μm) | -1.4 to -2.4 | -1.4 to -2.4 | -1.3 to -1.5 | -1.3 to -1.5 |
| Pixel size (Å) | 1.07 | 1.07 | 0.824 | 0.824 |
| Symmetry imposed | C4 | C4 | C4 | C4 |
| Initial particle images (no.) | 2,405,123 | 2,405,123 | 3,857,385 | 1,530,666 |
| Final particle images (no.) | 633,561 | 253,312 | 91,279 | 13,091 |
| Map resolution (Å) | 2.18 | 2.29 | 2.46 | 3.44 |
| FSC threshold | 0.143 | 0.143 | 0.143 | 0.143 |
| Map resolution range (Å) | 2.0-5.0 | 2.0-5.0 | 2.0-5.0 | 2.0-5.0 |
| **Refinement** | | | | |
| Initial model used (PDB code) | Alphafold prediction | Alphafold prediction | This study | This study |
| Model resolution (Å) | 2.23 | 2.58 | 2.56 | 3.75 |
| FSC threshold | 0.5 | 0.5 | 0.5 | 0.5 |
| Model resolution range (Å) | 2.1-2.2 | 2.2-2.6 | 2.4-2.6 | 3.2-3.7 |
| Map sharpening *B* factor (Å$^2$) | -59.1 | -55.7 | -68.8 | -41.0 |
| Model composition | | | | |
| Non-hydrogen atoms | 23,664 | 23,868 | 23,868 | 23,141 |
| Protein residues | 2,796 | 2,820 | 2,820 | 2,776 |
| Ligands | 28 | 24 | 20 | 29 |
| Nucleotide | 0 | 0 | 0 | 0 |
| *B* factors (Å$^2$) | | | | |
| Protein | 36.30 | 46.89 | 38.70 | 98.53 |
| Ligand | 45.89 | 67.75 | 31.49 | 105.44 |
| Nucleotide | 0 | 0 | 0 | 0 |
| R.m.s. deviations | | | | |
| Bond lengths (Å) | 0.004 | 0.005 | 0.002 | 0.004 |
| Bond angles (°) | 0.883 | 0.982 | 0.540 | 0.684 |
| Validation | | | | |
| MolProbity score | 1.39 | 1.52 | 1.43 | 1.76 |
| Clashscore | 7.00 | 10.05 | 7.85 | 9.84 |
| Poor rotamers (%) | 0.00 | 0.00 | 0.00 | 0.00 |
| Ramachandran plot | | | | |
| Favored (%) | 99.42 | 98.71 | 98.27 | 96.38 |
| Allowed (%) | 0.58 | 1.29 | 1.73 | 3.62 |
| Disallowed (%) | 0.00 | 0.00 | 0.00 | 0.00 |